Dynamic Interaction of S5 and S6 During Voltage-controlled Gating in a Potassium Channel

Felipe Espinosa, Richard Fleischhauer, Anne McMahon, and Rolf H. Joho

Center for Basic Neuroscience, The University of Texas Southwestern Medical Center, Dallas, TX 75390

ABSTRACT A gain-of-function mutation in the *Caenorhabditis elegans exp-2* K^+-channel gene is caused by a cysteine-to-tyrosine change (C480Y) in the sixth transmembrane segment of the channel (Davis, M.W., R. Fleischhauer, J.A. Dent, R.H. Joho, and L. Avery. 1999. *Science.* 286:2501–2504). In contrast to wild-type EXP-2 channels, homotetrameric C480Y mutant channels are open even at −160 mV, explaining the lethality of the homozygous mutant. We modeled the structure of EXP-2 on the 3-D scaffold of the K^+ channel KcsA. In the C480Y mutant, tyrosine 480 protrudes from S6 to near S5, suggesting that the bulky side chain may provide steric hindrance to the rotation of S6 that has been proposed to accompany the open-closed state transitions (Perozo, E., D.M. Cortes, and L.G. Cuello. 1999. *Science.* 285:73–78). We tested the hypothesis that only small side chains at position 480 allow the channel to close, but that bulky side chains trap the channel in the open state. Mutants with small side chain substitutions (Gly and Ser) behave like wild type; in contrast, bulky side chain substitutions (Trp, Phe, Leu, Ile, Val, and His) generate channels that conduct K^+ ions at potentials as negative as −120 mV. The side chain at position 480 in S6 in the pore model is close to and may interact with a conserved glycine (G421) in S5. Replacement of G421 with bulky side chains also leads to channels that are trapped in an active state, suggesting that S5 and S6 interact with each other during voltage-dependent open-closed state transitions, and that bulky side chains prevent the dynamic changes necessary for permanent channel closing. Single-channel recordings show that mutant channels open frequently at negative membrane potentials indicating that they fail to reach long-lasting, i.e., stable, closed states. Our data support a "two-gate model" with a pore gate responsible for the brief, voltage-independent openings and a separately located, voltage-activated gate (Liu, Y., and R.H. Joho. 1998. *Pflügers Arch.* 435: 654–661).

KEY WORDS: inward-rectifier • oocyte expression • mutant channels • two-gate hypothesis

INTRODUCTION

The *Caenorhabditis elegans* gene *exp-2* encodes a voltage-sensitive potassium (K^+) channel with an amino acid sequence related to Kv-type channels from *Drosophila* (*Shaker,* Shab, Shaw, and Shal) and vertebrates (Kv1–Kv9). Although the EXP-2 K^+ channel is structurally related to delayed-rectifier K^+ channels, it functions as an inward-rectifier with properties similar to the human *ether-à-go-go*–related gene (HERG)* channel (Fleischhauer et al., 2000). Unlike most Kv channels, which activate quite rapidly on membrane depolarization and remain open for prolonged periods at depolarized potentials, EXP-2 channels activate slowly ($\tau_{act} \sim 54$ ms at 20 mV) with a midpoint of activation at about −17 mV. In contrast to Kv channels, slow activation is followed by ultrafast inactivation ($\tau_{inact} < 1$ ms at >0 mV) leading to transient, small outward K^+ currents at positive potentials. Hence, although EXP-2 is clearly homologous to Kv-type delayed rectifier K^+ channels, it acts as an inward-rectifier with functional properties very similar to the structurally-unrelated HERG channel.

In *C. elegans*, several homozygous loss-of-function mutations in *exp-2* display dramatic broadening of the action potential (AP) in pharyngeal muscle cells and a concomitant slowing of the pumping of the pharynx (Davis et al., 1999). A gain-of-function mutation leads to brief pharyngeal APs in heterozygous worms and is lethal in homozygous worms. The mutant phenotype is caused by a cysteine-to-tyrosine change (C480Y) in S6 of EXP-2 (Davis, 1999; Davis et al., 1999). Homomeric C480Y mutant channels are open at potentials as negative as −160 mV, explaining the lethal nature of the homozygous mutation (Davis et al., 1999). In contrast to wild-type EXP-2 channels, heterotetrameric channels consisting of wild-type and mutant EXP-2 subunits begin to activate at about −70 mV (∼30 mV more negative than wild type). This may account for the narrow AP in heterozygous pharyngeal muscle.

To understand the molecular mechanism that may be responsible in keeping mutant EXP-2 channels from

Address correspondence to Dr. Rolf H. Joho, Center for Basic Neuroscience, The University of Texas Southwestern Medical Center, Dallas, TX 75390-9111. Fax: (214) 648-1801; E-mail: rolf.joho@utsouthwestern.edu

*Abbreviations used in this paper: AP, action potential; HERG, human *ether-à-go-go*–related gene; P_o, open probability.

closing at negative membrane potentials, we used the crystal structure of the KcsA K^+ channel (Doyle et al., 1998) as a scaffold to generate a 3-D model of the EXP-2 pore, including the transmembrane segments S5 and S6 (Davis et al., 1999). In this model, the large tyrosine side chain at position 480 in the C480Y mutant protrudes from S6 and projects toward S5 (see Fig. 1 B). In contrast, the much smaller cysteine side chain in the wild-type is buried close to S6 and is not in contact with S5. It was very interesting in this context that Perozo et al. (1999) had suggested that S6 may rotate counterclockwise (viewed from the outside) on KcsA channel opening. If the EXP-2 channel underwent a similar conformational change, then, in analogy to KcsA, the clockwise rotation of S6 that would be required for channel closing might be impaired due to steric hindrance in the presence of a bulky residue like tyrosine. Under this condition, the rotation of S6 required for long-lasting closings of the channel might not occur, not even at potentials as negative as −160 mV.

Here, we tested the hypothesis that S5 and S6 directly interact with each other during open-closed state transitions, and that only small side chains at position 480 in S6 allow EXP-2 K^+ channels to close. We find that EXP-2 channels with small side chains at position 480 in S6 (Gly, Ser, and Cys) behave like wild-type EXP-2. In contrast, bulky side chain substitutions (Tyr, Phe, and Trp) result in EXP-2 channels that allow large K^+ currents at negative potentials at which wild-type EXP-2 channels are closed. Side chains of intermediate size (Thr, Val, Leu, Ile, and His) define a third channel class with properties between wild-type channels and those permanently "trapped" in an open state. These findings suggest that S5 and S6 interact with each other during channel gating, and that bulky side chains at positions 421 in S5 or 480 in S6 generate steric hindrance and may prevent the postulated rotation of S6 required for stable channel closing.

MATERIALS AND METHODS

Synthesis of Wild-type and Mutant EXP-2 cRNA

The EXP-2 coding region (1,595 bp) inserted in the pT7 expression vector (a derivative of pSP64) was used to generate cRNA for channel expression in *Xenopus* oocytes (Fleischhauer et al., 2000). This vector contains a T7 promoter, 44 bases of the *Xenopus* β-globin 5′ untranslated region, and 143 bases of the *Xenopus* β-globin 3′ untranslated region followed by a poly-A tract. The construct was linearized with BamHI and in vitro transcription was performed using the Ribomax T7 kit (Promega) to generate a cRNA 2,134 nucleotides long. Capped transcripts were produced by the addition of 3 mM $m^7G(5')ppp(5')G$ (New England Biolabs) to the reaction (Zühlke et al., 1995). Mutations in EXP-2 cDNA were generated using the QuickChange site director mutagenesis kit (Stratagene). All mutant cDNAs were completely sequenced to verify the absence of undesired mutations.

Electrophysiology

Approximately 1–3 ng cRNA was injected into *Xenopus laevis* oocytes. After 1–4 d at 16°C, cells were subjected to a standard two-electrode voltage-clamp protocol (VanDongen et al., 1990; Fleischhauer et al., 2000) using an amplifier (model OC-725A; Warner Instruments Corp.). Experiments were done at room temperature (22 ± 1°C) in the following solution containing (in mM): 100 KCl, 1 $MgCl_2$, and 1.8 $CaCl_2$ in 5 HEPES, pH 7.4. Both voltage-sensing and current-passing electrodes were filled with 3 M KCl and had resistances of 0.2–1.0 MΩ. The pCLAMP 6.0 software (Axon Instruments Inc.) was used to generate voltage-pulse protocols and for data acquisition. Signals were filtered at 0.5–2.0 kHz and digitized at 1–10 kHz. Capacitive and leakage currents were not subtracted, and membrane potentials were not corrected for series resistance errors.

For single-channel recordings, experiments were essentially done as described previously (Moorman et al., 1990; Liu and Joho, 1998). Oocytes were kept in the following solution (in mM): 100 KCl, 1.0 $MgCl_2$, and 5.0 HEPES, pH 7.4. The pipette contained the following (in mM): 100 KCl, 1.0 $MgCl_2$, 1.8 $CaCl_2$, and 5.0 HEPES, pH 7.4, unless otherwise indicated. Analogue signals were filtered at 2 or 10 kHz (Axopatch 200A and pCLAMP version 6.0, Axon Instruments Inc.), digitized at 25 or 50 kHz, and stored for offline analysis.

Data Acquisition and Analysis

Single-channel data were analyzed using Fetchan and pSTAT (pCLAMP 6.0). For dwell-time distributions, a bin width of 0.04 ms was used. Mono- and double-exponential functions were fit by minimizing the mean squares of the errors using an iterative algorithm.

RESULTS

Bulky Side Chains at Position 480 in S6 Interfere with Voltage-dependent Channel Closing

The SWISS-MODEL server (www.expasy.ch/swissmod/SWISS-MODEL.html) is an automated system that generates a putative structure of a new sequence based on an experimentally determined structure using energy minimization and molecular dynamics (Guex and Peitsch, 1997). We used the crystal structure of the KcsA K^+ channel (Doyle et al., 1998) as a scaffold to generate a 3-D model of the EXP-2 pore, including the transmembrane segments S5 and S6 (Davis et al., 1999). Fig. 1 shows the relevant amino acid sequence of EXP-2 and the corresponding putative pore structure for the wild-type and the C480Y mutant channels. The SWISS-PDB Viewer was used to generate the C480Y mutant structure by substituting tyrosine for cysteine and selecting the lowest energy rotamer. In this model structure, it is apparent that the large tyrosine side chain in the C480Y mutant protrudes from S6 and projects toward, and possibly makes contact with, S5. In contrast, the smaller cysteine side chain is buried close to S6 without contacting S5 (Fig. 1 B). Based on the channel-gating model proposed by Perozo et al. (1999), we assumed that the S6 segment in EXP-2 might rotate counterclockwise on K^+ channel opening and clockwise on closing. Because we

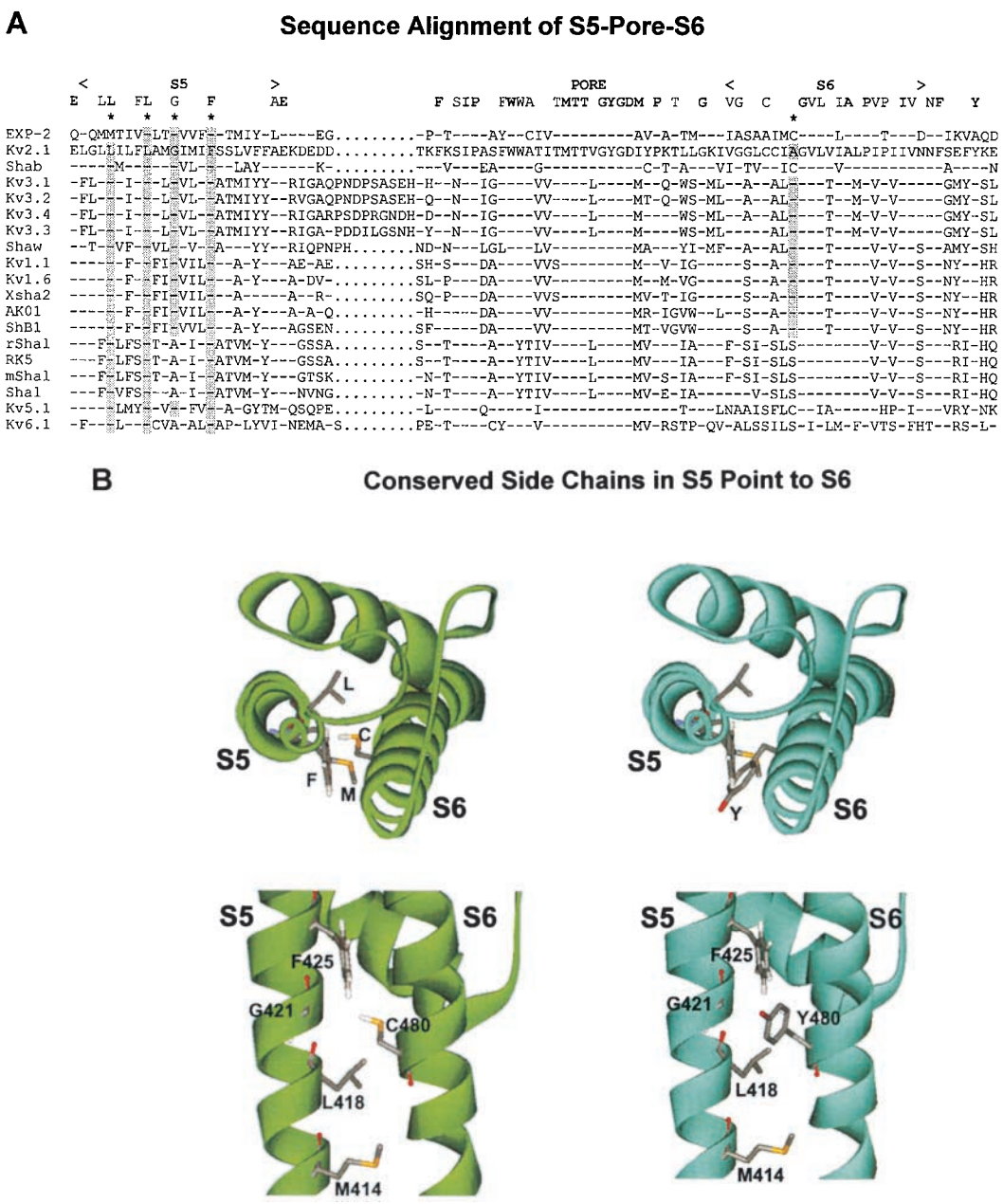

FIGURE 1. S5-Pore-S6 alignment and pore model of EXP-2. (A) Sequence alignment for the S5-pore-S6 region of several K^+ channels from different Kv subfamilies. The side chains highlighted by asterisks above the EXP-2 sequence are drawn as sticks in B. ("-" indicates identity to the sequence of Kv2.1; "." indicates a gap required to maintain alignment. Conserved amino acids are shown by letters on the top; residues that are absolutely conserved in Kv channels are in bold.) (B) Top and side views of the S5-pore-S6 region of EXP-2. The four conserved side chains in S5 that are marked by asterisks (M414, L418, G421, and F425) are on the same side of the S5 helix and project toward S6. The side chain at position 480 in S6 points toward the conserved G421 that is flanked by L418 and F425 in S5. The model suggests possible interaction between G421 in S5 and the side chain at position 480 in S6. In case of an aromatic side chain at position 480, there may be aromatic–aromatic interaction with the invariant F425 in S5.

had previously shown that the C480Y mutant was trapped in an open state (Davis et al., 1999), we hypothesized that the bulky tyrosine side chain may prevent the clockwise rotation of S6 required to close the channel completely and permanently.

To test this hypothesis, we replaced cysteine 480 in S6 with a series of amino acids that differed widely in size, polarity, and aromaticity. cRNA encoding wild-type or mutant EXP-2 channel was injected in *Xenopus* oocytes, and the resulting K^+ currents were measured using a standard two-electrode voltage-clamp protocol (VanDongen et al., 1990; Fleischhauer et al., 2000). Oocytes, in 100 mM KCl in frog Ringer to facilitate the measurement of inward currents, were held at −120 mV. Upon

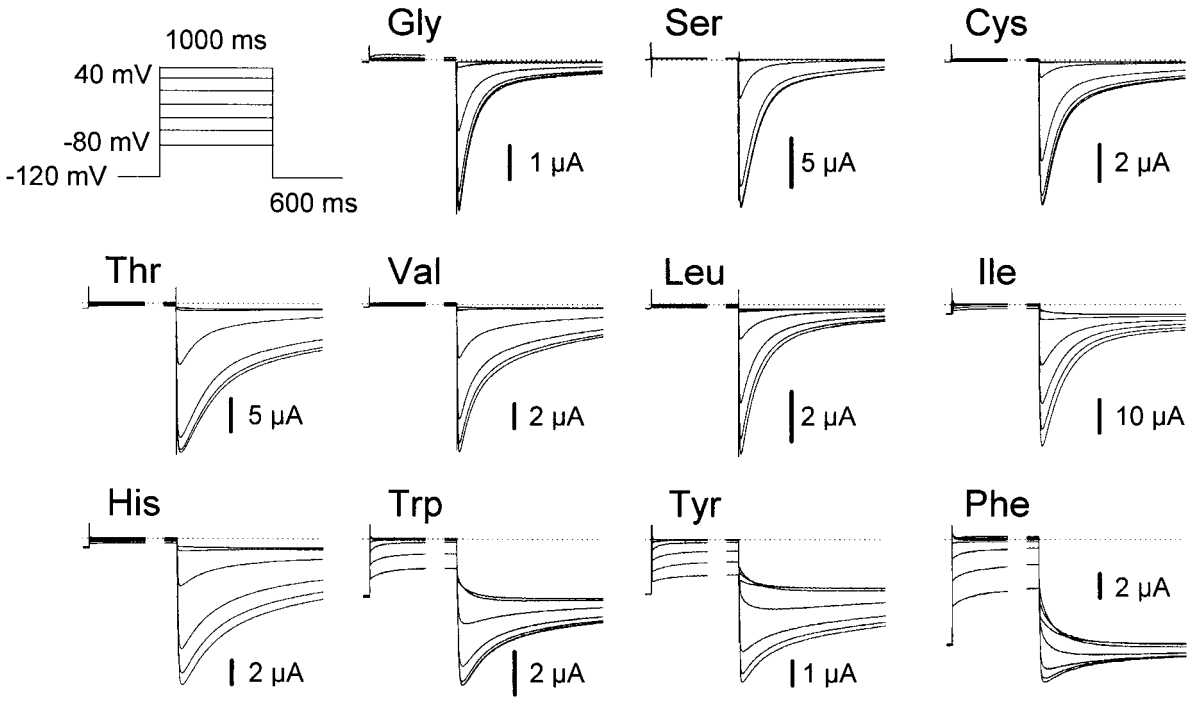

FIGURE 2. Bulky side chains at position 480 in S6 trap EXP-2 channels in an open state. Bulky side chains prevent EXP-2 channels from fully closing, indicated by large steady-state inward currents at −120 mV. Oocytes (in 100 mM KCl containing Ringer) were held at −120 mV and subjected to 1-s depolarizing pulses in 20-mV increments from −80 to 40 mV (only the beginning part of the 1-s pulse is shown), followed by 600-ms pulses to −120 mV. Neither wild-type nor mutant channels show measurable outward currents, indicating fast inactivation ($\tau_{inact} < 1$ ms at 20 mV for wild-type EXP-2). When small side chains (Gly, Ser, and Cys) occupy position 480, channels show tail currents that approach zero after a few hundred milliseconds. For bulky side chain substitutions (Phe, Tyr, and Trp), channels incompletely deactivate at −120 mV, which is indicated by substantial tail currents that do not reach zero.

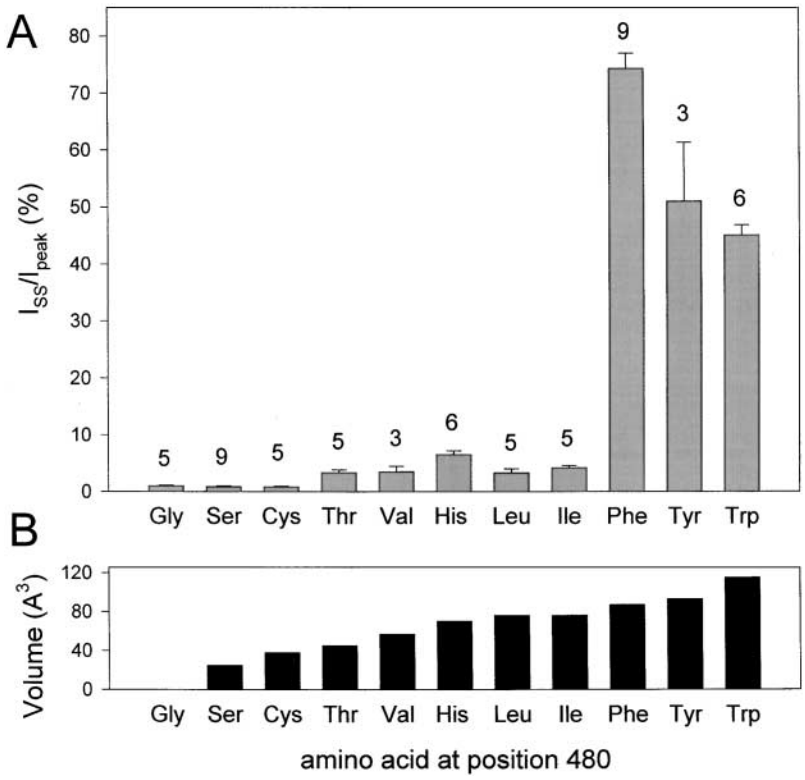

FIGURE 3. Bulky, aromatic side chains prevent channel closing. The ratio of steady-state current at −120 mV (I_{SS}) to maximal tail current (I_{peak}) increases with side chain volume and aromaticity at position 480 in S6. The side chain volumes are from Zühlke et al. (1994).

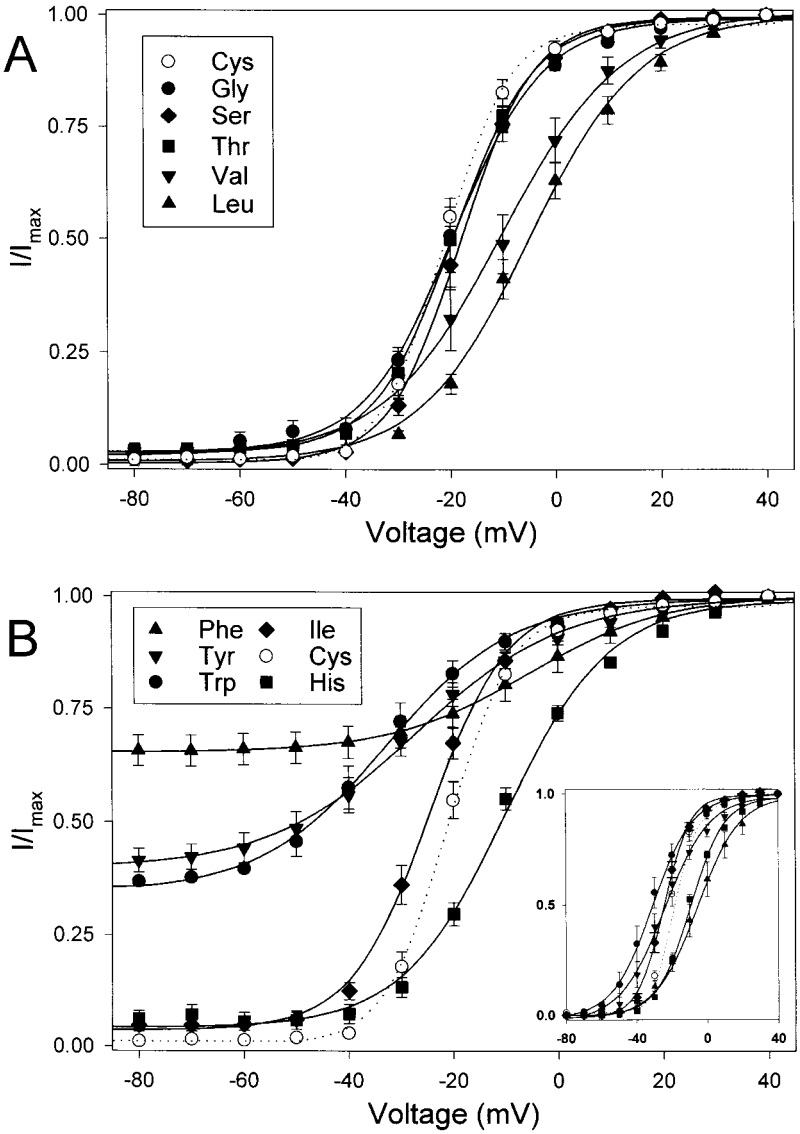

FIGURE 4. Voltage dependence of S6 mutants. (A) G-V relationships are shown for those S6 mutations (Gly, Ser, Thr, Val, and Leu) that do not lead to large steady-state currents (I_{SS}) at −120 mV. (B) G-V relationships are shown for S6 mutations (His, Ile, Trp, Tyr, and Phe) that lead to increasingly larger I_{SS}/I_{peak} ratios at −120 mV. The G-V curve for wild-type C480 is shown as a dotted line in A and B. Oocytes were held at −120 mV, and 1-s test pulses to potentials from −80 to 40 mV were applied in 10-mV increments, followed by 200-ms pulses to −120 mV. The peaks of the resulting tail currents were normalized to the maximal current. The G-V relationships were fit to a Boltzmann equation, and the midpoints of activation and the slope factors *k* were calculated (listed in Table I). The inset in B shows the G-V curves when I_{SS} at −120 mV is subtracted. The symbols show means ± SEM (three to seven oocytes).

depolarization for 1 s to 40 mV, no significant outward currents could be detected neither for wild-type nor mutant EXP-2 channels (Fig. 2) because of ultrafast inactivation at positive potentials (wild-type EXP-2 inactivates with a $\tau_{inact} < 1$ ms at 20 mV; Fleischhauer et al., 2000). When the oocyte membrane was repolarized to −120 mV, large transient inward tail currents appeared that declined toward zero current for the wild-type C480 and the mutants C480G and C480S. For wild-type EXP-2, we had shown that these tail currents arose from rapid voltage-dependent recovery from inactivation ($\tau_{rec} \sim 1$ ms at −120 mV) followed by relatively slow channel deactivation ($\tau_{deact} \sim 80$ ms at −120 mV; Fleischhauer et al., 2000). In contrast to the mutants carrying small side chain substitutions, the C480F and C480W mutants behaved very differently. Their tail currents approached plateau values clearly different from zero, similar to our previous finding with the C480Y mutant (Davis et al., 1999). Particularly for the mutant C480F, channel deactivation proceeded very slowly and the current at steady state was ~75% of the peak of the tail current. A third class of mutants (C480T, C480V, C480L, C480I, and C480H) differed from the two classes described so far. The tail currents of these mutants decayed toward, but did not reach, zero. The steady-state current levels were clearly different from those of C480G, C480S, and wild-type EXP-2 (Fig. 2).

To quantify and compare these observations, we used the ratio of steady-state inward current (I_{SS}) at −120 mV to the peak of the tail current at −120 mV (after a 1-s depolarizing pulse to 40 mV to activate and inactivate the channels). As seen in Fig. 3 A, there are three distinct groups characterized by different levels of I_{SS} at −120 mV. Group 1 channels (Gly, Ser, and Cys) are wild-type-like, i.e., there was no measurable EXP-2-specific I_{SS} at −120 mV (when corrected for oocyte leak),

TABLE I

Time Constants of Activation and Recovery from Inactivation and Deactivation

	$E_{0.5}$	Slope	Activation at 20 mV	Recovery	Deactivation at −120 mV
	mV	*ms*	*ms*	*ms*	*ms*
C480	−17 ± 2	6.5 ± 0.3 (5)	54 ± 5 (10)	1.1 ± 0.1 (5)	64 ± 8.8 (0.58); 391 ± 73 (0.38) (4)
C480G	−19 ± 0.7	8.0 ± 0.2 (6)	77 ± 10 (6)	nd	56 ± 0.8 (0.69); 289 ± 14 (0.27) (6)
C480S	−18 ± 1.4	7.0 ± 0.2 (6)	74 ± 17 (8)	1.5 ± 0.1 (8)	58 ± 0.9 (0.68); 277 ± 6.8 (0.30) (5)
C480T	−19 ± 2.3	8.0 ± 0.5 (3)	79 ± 10 (3)	nd	76 ± 1.5 (0.44); 347 ± 9.6 (0.47) (3)
C480V	−10 ± 6.9	11 ± 0.8 (4)	123 ± 40; 980 ± 33 (3)	nd	77 ± 3.6 (0.37); 497 ± 11 (0.31) (3)
C480L	−5.0 ± 2.2	11 ± 0.2 (5)	172 ± 24; 1,672 ± 155 (5)	1.5 ± 0.1 (4)	61 ± 0.5 (0.56); 265 ± 10 (0.34) (5)
C480I	−25 ± 1.5	12 ± 1.8 (5)	90 ± 16; 1,642 ± 175 (5)	1.3 ± 0.2[a] (4)	87 ± 1.4 (0.48); 869 ± 44 (0.35) (5)
C480H	−9.0 ± 0.9	10 ± 0.2 (5)	143 ± 7 (6)	2.1 ± 0.1[a] (4)	99 ± 1.2 (0.28); 406 ± 21 (0.48) (5)
C480Y	−24 ± 2.7	13 ± 1.2 (5)	101 ± 3; 1,353 ± 64 (5)	nd	85 ± 4.6 (0.19); 795 ± 29 (0.38) (3)
C480W	−31 ± 3.6	10 ± 0.4 (6)	131 ± 24; 1,627 ± 203 (5)	nd	98 ± 2.8 (0.35); 524 ± 25 (0.24) (7)
C480F	−6.0 ± 4.4	12 ± 1.7 (7)	317 ± 50; 2,865 ± 368 (7)	1.1 ± 0.2[a] (8)	97 ± 1.2 (0.17); 424 ± 34 (0.14)[a] (7)

The time constants for activation (at 20 mV), recovery from inactivation (at −120 mV) and deactivation (at −120 mV) are listed (mean ± SEM, number of oocytes in parenthesis; n.d. = not determined). For recovery from inactivation, $\tau 2$ = 3.0 ± 0.4 ms for C480I, 4.8 ± 1.3 ms for C480H and 4.2 ± 0.4 ms for C480F. For deactivation, two exponentials and their relative contributions are listed. For small side chains, two exponentials describe deactivation reasonably well; for larger side chain substitutions, additional exponentials with time constants in the range of seconds to minutes are required (only determined for C480F, $\tau 3$ = 3.5 ± 0.6 s [n = 6], and $\tau 4$ = 423 ± 77 s [n = 4]).

[a]Indicates the requirement of additional exponentials.

and these channels were closed at −120 mV. Group 2 channels (Thr, Val, His, Leu, and Ile) represent mutant channels that showed small but significant I_{SS} at −120 mV (3–7% of peak tail currents). Finally, group 3 channels (Phe, Tyr, and Trp) showed large I_{SS} (45–75% of peak tail currents) under these conditions. It is apparent that the ratio of I_{SS}/I_{peak} at negative potentials correlates with side chain volume and, particularly, with aromaticity at position 480 (Fig. 3 B).

Voltage Dependence and Activation-Deactivation Kinetics Are Altered in Mutant EXP-2 Channels

We used the peak values of the tail currents to determine the G-V relationship of wild-type and mutant EXP-2 channels (Fig. 4). The mutants C480G, C480S, and C480T showed G-V curves virtually identical to that of the wild-type C480. The introduction of the somewhat larger side chains of Val, Leu, and His shifted the midpoints of activation by ∼10 mV in the depolarizing direction (Fig. 4, A and B, and Table I). In contrast, the midpoints of activation for the β-brancher Ile (same side chain volume like Leu) and for the aromatic side chains Tyr and Trp were shifted ∼10–15 mV in the hyperpolarizing direction compared with wild-type C480 (Fig. 4 B and Table I). For the mutant C480F, which showed the largest steady-state current at −120 mV, the midpoint of activation was again shifted ∼10 mV toward more positive potentials (Fig. 4 B and Table I).

We used a two-pulse protocol to determine the kinetics of activation of wild-type and mutant EXP-2 channels (Fig. 5 A). EXP-2-expressing oocytes were subjected for different times to depolarizing pulses to 20 mV to activate and inactivate the channels. The fraction of activated/inactivated channels was measured by subsequent 600-ms test pulses to −120 mV. We had shown previously that wild-type EXP-2 channels activate relatively slowly (τ_{act} = 54 ± 5 ms at 20 mV [n = 10]) compared with other Kv-type K^+ channels. The Gly-, Ser- and Thr-substituted EXP-2 channels activated with similar kinetics (τ_{act} at 20 mV: 77 ± 10 ms [n = 6], 74 ± 17 ms [n = 8], and 79 ± 10 ms [n = 3] for C480G, C480S, and C480T, respectively). In contrast, the increase of current for the C480F mutant (beyond the steady-state current already present at −120 mV) developed much more slowly. It took several seconds to approach complete activation, and the time course was better fit by two exponentials (at 20 mV: $\tau 1_{act}$ = 317 ± 50 ms; $\tau 2_{act}$ = 2,865 ± 368 ms [n = 7]). The other channel mutants activated with kinetics that were intermediate between wild-type C480 and the C480F mutant (Fig. 5 A and Table I).

The current traces shown in Fig. 2 suggested that deactivation may also be changed in several EXP-2 mutants when compared with wild-type. When the induced tail currents (at −120 mV) were normalized for direct visual comparison (after subtraction of I_{SS}), it was apparent that, for the most part, EXP-2 channels with small side chains at position 480 deactivated more rapidly than EXP-2 channels carrying larger side chain substitutions (Fig. 5 B). For the mutants with smaller side chains, we could describe deactivation kinetics reasonably well with two exponentials; however, for larger side chain substitutions, we needed additional exponentials with τ_{deact} values in the range of many seconds to minutes to obtain adequate fits (only accurately determined

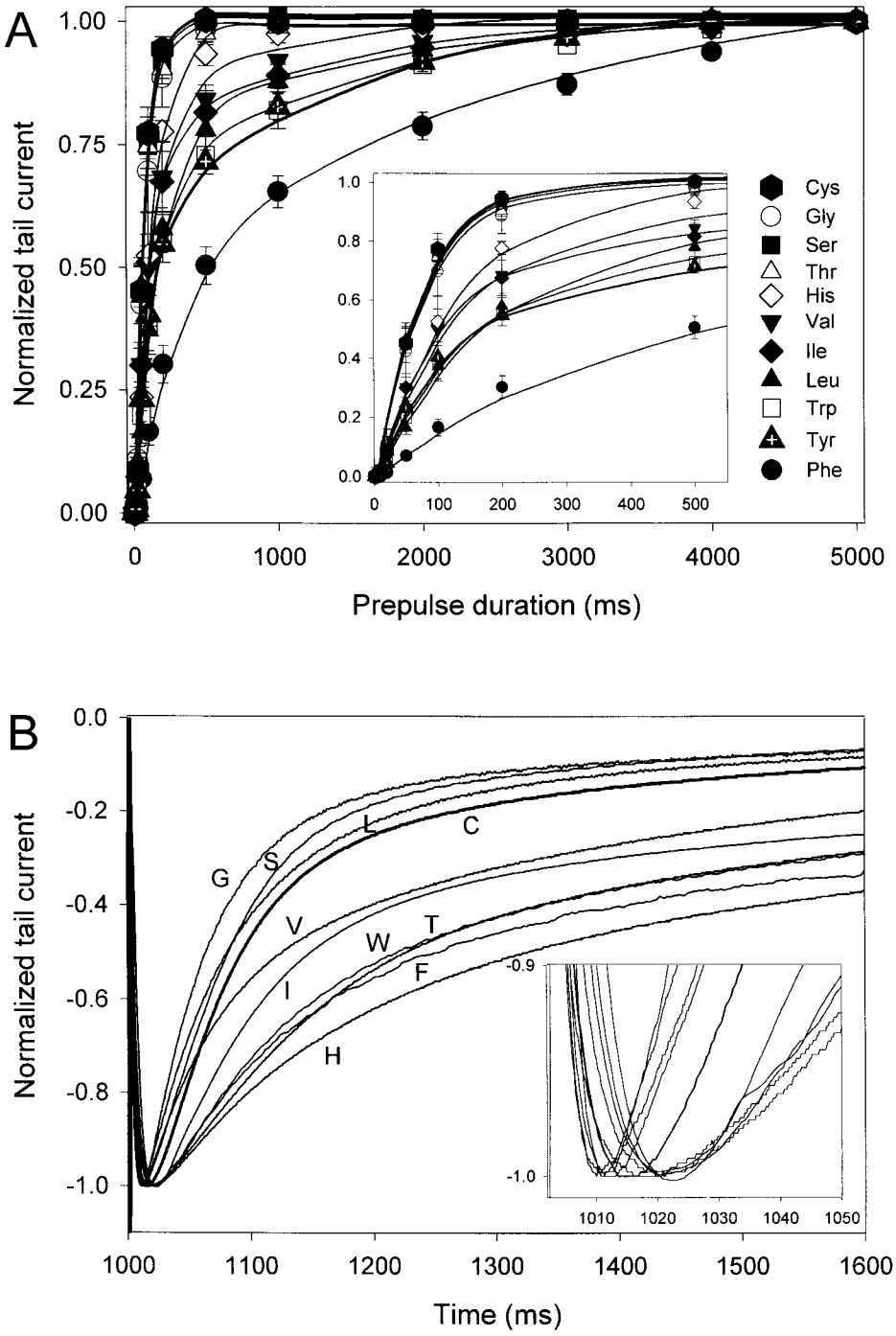

FIGURE 5. Kinetics of activation and recovery from inactivation and deactivation. (A) Oocytes were held at −120 mV, and test pulses to 20 mV were applied lasting from 1 to 5,000 ms. The time dependence of activation was determined from the peak tail currents during the subsequent pulses to −120 mV. (B) EXP-2 channels were activated/inactivated by 1-s prepulses to 20 mV, and then 600-ms test pulses to −120 mV were applied to initiate recovery from inactivation followed by deactivation. Tail currents were normalized (0 corresponds to I_{SS} at −120 mV; −1 corresponds to the peak of the tail current). The inset shows small differences in the kinetics of recovery from inactivation.

for C480F). The deactivation time constants for wild-type and mutant EXP-2 channels are shown in Table I.

In contrast to the relatively big changes between wild-type and mutant channels in the kinetics of activation and deactivation, there were relatively small changes in the kinetics of recovery from inactivation. All channels described in Fig. 2 showed rapidly rising tail currents at −120 mV due to fast recovery from inactivation, and there were only small differences between wild-type and the various mutant EXP-2 channels (Fig. 5 B and Table I). We have not quantitatively analyzed the inactivation kinetics of the mutant EXP-2 channels, but it appears from Fig. 2 that there are no obvious differences between wild-type and mutant channels. Like wild-type EXP-2 ($\tau_{inact} < 1$ ms at 20 mV; Fleischhauer et al., 2000), mutant channels show no outward currents during the 1-s activation period. (A more quantitative analysis of inactivation kinetics would require the use of the cut-open oocyte technique to obtain an adequate fast voltage clamp and is beyond the scope of this work.)

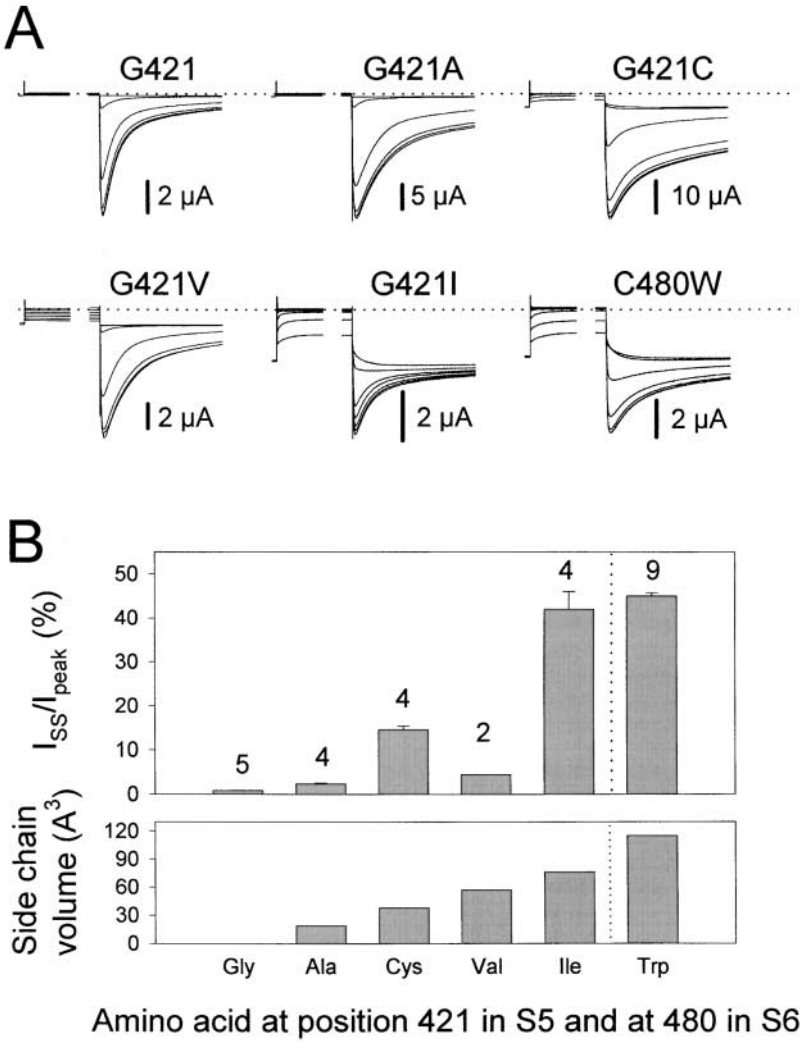

FIGURE 6. Mutations in S5 trap the channel in an active state. (A) Oocytes (in 100 mM KCl containing Ringer) were held at −120 mV and subjected to 1-s depolarizing pulses in 20-mV increments from −80 mV to 40 mV, followed by 600-ms pulses to −120 mV (as described Fig. 2 legend). Replacement of the conserved G421 in S5 with larger side chains prevents EXP-2 channels from closing similar to the mutations at position 480 in S6. (B) The I_{SS}/I_{peak} ratio at −120 mV increases with the side chain volume at position 421 in S5.

S5–S6 Interaction during Gating Transitions

The findings with the S6 mutants were in agreement with our hypothesis that bulky side chains at position 480 in S6 interfere with S6 rotation, a mechanism proposed for KcsA channel gating (Perozo et al., 1999). side chain bulkiness and, particularly, aromaticity at position 480 correlated well with the I_{SS}/I_{peak} ratio at negative potentials (Fig. 3 B).

The 3-D model structure of EXP-2 shows that the side chains in S5 pointing toward S6 are highly conserved in channels representing different Kv subfamilies (Fig. 1 A). The S5 residues M414, L418, G421, and F425 are positioned on the conserved side of S5 pointing toward S6 (Fig. 1 B). L418 and F425 are invariant residues in the Kv channels listed in Fig. 1 A; M414 and G421 show only very conserved substitutions (Met for Leu at position 414, Ala for Gly at position 421). In the model, the bulky tyrosine side chain at position 480 in S6 projects to, and may interact with, G421 in S5, which is flanked by the conserved L418 and F425 (Fig. 1 B). Because G421 appeared close to C480, we considered it possible that larger side chains at position 421, in analogy to bulky side chains at position 480, might also trap the channel in a state from which it cannot close.

We tested this hypothesis by gradually increasing the side chain volume at position 421 in S5. Compared with wild-type EXP-2, deactivation was slowed for the G421A mutant, and the inward tail currents at −120 mV approached, yet did not reach, zero (Fig. 6). The mutants G421C and G421V deactivated even more slowly than G421A. The mutant G421I showed the biggest difference. A large I_{SS} remained at −120 mV (~50% of the peak tail current). The current traces for G421I looked very similar to those obtained for the S6 mutant C480W. These results are in agreement with a model where the side chain at position 421 in S5 is close to and interacts with the side chain at position 480 in S6 (Fig. 1 B).

Although the I_{SS}/I_{peak} ratio correlated with side chain volume at position 480 in S6, it was aromaticity that seemed to be particularly important (Figs. 2 and 3). The model structure for the C480Y mutant (Fig. 1 B, right panel) suggests a possible explanation for this finding. It appears that the side chain of tyrosine 480 projects toward the invariant F425 in S5, and may participate in ar-

omatic–aromatic interaction which, in turn, could have a stabilizing effect on a particular channel conformation (Burley and Petsko, 1985). We tested the possibility of aromatic–aromatic interaction by changing the invariant F425 in S5 to either alanine or isoleucine in the wild-type background and in the S6 mutants C480L, C480I, C480H, C480F, and C480W. The I_{SS}/I_{peak} ratio was reduced from 74.3 ± 2.7% ($n = 9$) for the double mutant F425A/C480F to 43.6 ± 1.3% ($n = 9$) for the single mutant F425/C480F. Likewise, the I_{SS}/I_{peak} ratio for F425A/C480W was reduced from 45.1 ± 1.8% ($n = 6$) to 34.0 ± 2.5% ($n = 4$) for F425/C480W. The double mutants F425A/C480L, F425A/C480I, F425A/C480H, and all F425I-containing double mutants did not result in functional K^+ channels in oocytes (no measurable currents). The fact that the double mutants F425A/C480F and F425A/C480W compared with the F425-containing single mutants show reduced I_{SS}/I_{peak} ratios is in agreement with the notion that aromatic–aromatic interaction between F425 in S5 and the aromatic side chain at position 480 in S6 stabilizes a channel conformation from which EXP-2 cannot easily close.

Mutant EXP-2 Channels Show Bursts of Openings at Negative Potentials

So far, our data agree with the hypothesis that S5 and S6 segments interact during voltage-dependent gating, possibly while S6 is moving during closed-open state transitions, and that interference with the proposed rotation of S6 prevents the voltage-activated gate from closing. It is conceivable that the S6 segment in the C480Y mutant rotates enough for channels to close briefly but that the presence of the bulky tyrosine side chain at position 480 destabilizes the closed state and facilitates closed-open state transitions. Such a mechanism might lead to an open probability (P_o) greater than zero, even at very negative membrane potentials. At least two different mechanisms could account for the observed steady-state current at negative potentials: (1) P_o of mutant channels may not approach zero even at membrane potentials as negative as −160 mV with no change in the unit conductance (γ) of mutant channels; or (2) mutant channels could enter different subconductance states at negative potentials (with $P_o > 0$). To distinguish between these two possibilities, we recorded single-channel activity of wild-type, C480I (intermediate I_{SS}), and C480F (large I_{SS}) mutant channels during the first 200 ms after recovery from inactivation (encompassing the peak of the macroscopic tail current) and 3 s later during deactivation when channels approached steady-state conditions.

Fig. 7 shows single-channel activity in cell-attached patches of C480 wild-type and C480I and C480F mutant channels. During the first 200 ms after repolarization to −80 mV (after recovery from inactivation), no obvious differences could be seen in kinetics and single-

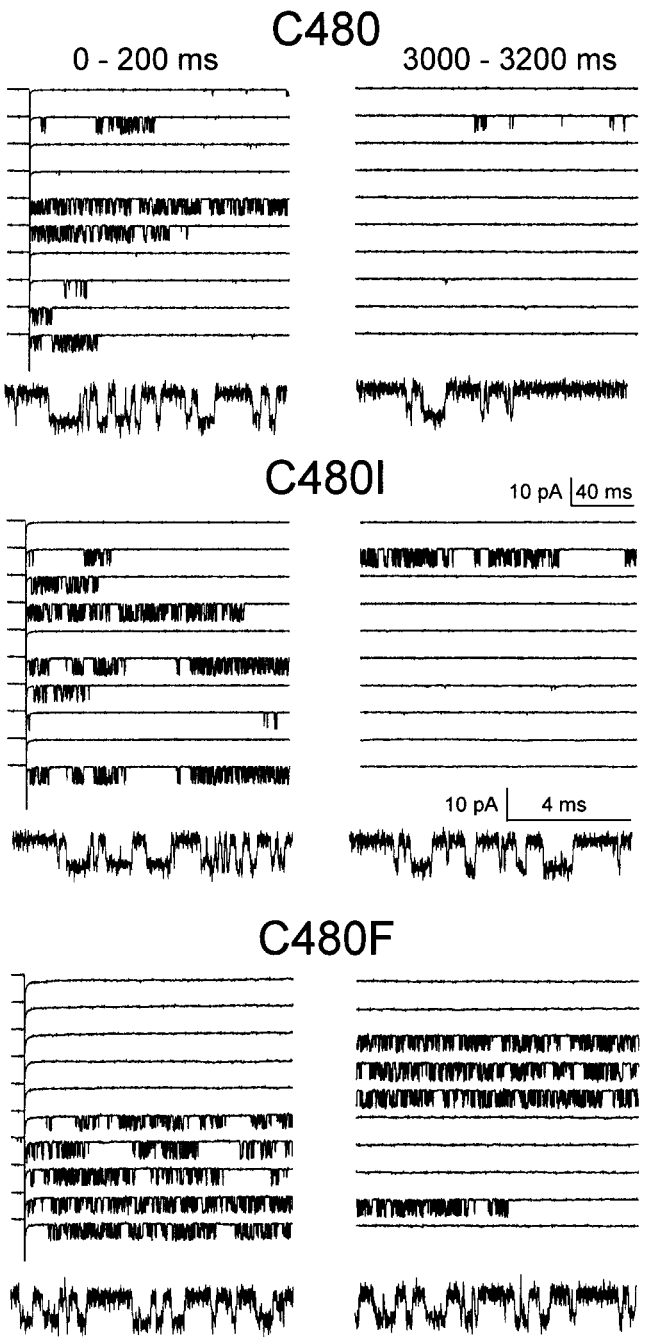

FIGURE 7. Single-channel activity of wild-type C480 and mutants C480I and C480F. Channels were activated-inactivated from a holding potential of −80 mV by 1-s pulses to 20 mV; the voltage was then returned to −80 mV to allow recovery from inactivation followed by deactivation. The 10 consecutive current traces on the left represent the first 200 ms after repolarization to −80 mV. The expanded traces (10-ms duration) show similar kinetics and single-channel currents for the wild-type and the mutant channels. On the right, 10 consecutive 200-ms current traces were recorded 3 s after the beginning of repolarization when the tail currents had reached near steady-state levels (<1% for wild-type EXP-2, ~5% for C480I and ~75% of the peak tail current for C480F; Fig. 3 A). As expected from macroscopic current measurements, wild-type EXP-2 shows mainly null traces. In contrast, the C480F mutant shows single-channel activity similar to the activity seen at the peak of the tail current. The C480I mutant shows behavior between wild-type and C480F. Currents were low-pass filtered at 2 and 10 kHz, and digitized at 25 and 50 kHz for the recordings shown in the 200-ms and 10-ms traces, respectively.

channel current amplitudes between wild-type and mutant channels (Fig. 7, left panels). For the wild-type and both mutants, many test pulses to −80 mV resulted in traces without channel openings. We used 1-s activating pulses, therefore, most channels should have been activated, then inactivated (τ_{act} = 54 ± 5 ms at 20 mV for wild-type EXP-2), and be ready to recover from inactivation during the test pulses to −80 mV. The fact that we saw a large fraction of null traces (~50–70%) suggests that EXP-2 channel may recover from inactivation without entering the open state.

Measuring single-channel activity 3 s into the repolarizing test pulse, however, revealed big differences among the different channels (Fig. 7, right panels). Under these conditions, the corresponding macroscopic tail currents would have approached steady-state levels (<1% current for wild-type EXP-2, ~5% and ~75% of the peak tail currents for C480I and C480F, respectively; Figs. 2 and 3 A). As expected from the macroscopic current measurements, wild-type EXP-2 showed mainly null traces; only infrequently did we observe a trace with single-channel activity. In stark contrast, the C480F mutant showed many traces with long bursts of single-channel activity. For C480F, these bursts appeared to be as frequent as those during the first 200 ms of the repolarizing test pulse. For the C480I mutant, we saw fewer traces with single-channel activity than for C480F. Importantly, for the three channels studied, we did not see any obvious changes in single-channel current amplitude (Fig. 7, expanded traces). This indicates that the macroscopic steady-state currents seen in the S6 mutants are caused by bursts of channel reopenings at negative membrane potentials.

The expanded current traces for C480, C480I, and C480F suggested that there were no big changes in the open times and brief, intraburst closed times among the studied channels (Fig. 7). The open- and closed-time histograms confirmed the initial impression (Fig. 8). Although there were dramatic differences in P_o, corresponding to the large changes in I_{ss}, there were little or no differences in mean open times and mean intraburst closed times. The distribution of open times for C480, C480I, and C480F could be well fit with single exponentials yielding mean open times of 0.24 ± 0.01 ms (n = 7), 0.20 ± 0.02 ms (n = 4), and 0.22 ± 0.01 ms (n = 6) for C480, C480I, and C480F, respectively. The closed time distributions (determined from the 200-ms recordings) could be better fit with two exponentials. The mean closed times were ~0.1 ms and ~0.6 ms for wild-type and mutant channels.

DISCUSSION

EXP-2 is a voltage-gated, Kv-type K^+ channel that is involved in the repolarization phase of the AP in the pharyngeal muscle of *C. elegans* (Davis et al., 1999). Although the EXP-2 K^+ channel is structurally related to delayed rectifier K^+ channels (~40% amino acid sequence identity to all Kv-type channels), it is functionally distinct (Fleischhauer et al., 2000). In response to depolarization, EXP-2 channels activate slowly and inactivate very rapidly (τ_{inact} < 1 ms at 20 mV). Upon repolarization, recovery from inactivation is also fast and strongly voltage dependent. These kinetic properties make the Kv-type EXP-2 channel an inward-rectifier that resembles functionally the structurally completely unrelated HERG channel (Fleischhauer et al., 2000). The C480Y gain-of-function mutation leads to brief pharyngeal APs in heterozygous *C. elegans,* and is lethal in homozygous worms (Davis, 1999; Davis et al., 1999). We showed previously that homomeric C480Y mutant channels remain open at potentials as negative as −160 mV, explaining the lethal nature of this mutation (Davis et al., 1999).

Bulky Side Chains in S6 Prevent the Channel from Closing

It was shown that counterclockwise rotation of the S6 segment accompanies opening of the KcsA K^+ channel (Perozo et al., 1999). If a similar gating mechanism applied to EXP-2, then clockwise rotation of the S6 segment would be required for channel closing. Hence, the presence of a bulky side chain at position 480 in S6 of EXP-2 could partially or fully prevent this rotation and trap the channel in the open state (Fig. 1 B). To test this hypothesis, we replaced the small cysteine side chain at position 480 with side chains differing in size, polarity, and aromaticity. We found that channel mutants with small side chain substitutions (Gly and Ser) behave like wild type; in contrast, substitutions of larger side chains at position 480 (Trp, Phe, Leu, Ile, and Val) lead to mutant channels that are open and conduct K^+ ions at potentials as negative as −120 mV (Fig. 2). Although the extent of the steady-state current (I_{SS}) at negative potentials correlates with the side chain volume at position 480, aromaticity seems to be particularly important. There appear to be two "thresholds" at which the behavior of mutant channels changes rather abruptly: (1) at side chain volumes >38 A^3, separating Cys from Thr, EXP-2 channels no longer close permanently, leading to small I_{SS} (3–7% of maximal tail currents); and (2) the introduction of aromatic side chains induces dramatic changes leading to large I_{SS} (45–75% of peak; Fig. 3 B).

S5–S6 Interaction during Channel Gating

The S5 segment of Kv-type K^+ channels contains several absolutely conserved amino acid residues (Fig. 1 A). The conserved S5 residues M414, L418, G421, and F425 in EXP-2 are positioned on the side facing and possibly interacting with S6 (Fig. 1 B). The side chain at position 480 in S6 projects toward G421, which is flanked by the invariant L418 and F425. In the 3-D pore model, the S5

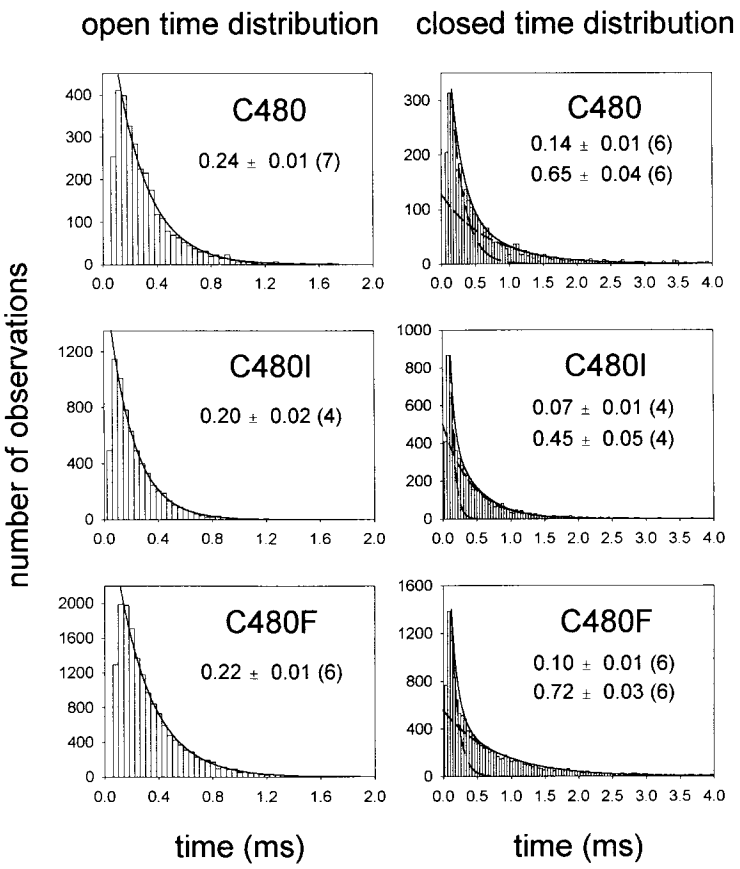

FIGURE 8. Open and closed times are not significantly affected by mutations in S6. Histograms of open and closed times show no differences between C480 wild-type and C480I and C480F mutant channels. Open-time distributions were fit with single exponentials, closed-time distributions with two exponentials. The mean open and closed times in milliseconds (mean ± SEM) and the number of experiments are shown for each channel.

residue G421 is close to C480 in S6, and we predicted that bulky side chains at position 421—similar to those at position 480—may also trap the channel in an open state. Indeed, when we tested this hypothesis by gradually increasing the side chain volume at position 421 in S5, we found large steady-state currents at −120 mV for mutant channels carrying intermediate-sized side chains at position 421 in S5 (Fig. 6).

Although the side chain of phenylalanine (87 A^3) is not much more voluminous than that of isoleucine or leucine (76 A^3), it obviously has a much more dramatic effect, indicating that the aromatic nature of the side chain in S6 may play a particularly important role in keeping the mutant channels from closing. Visual inspection of Fig. 1 B suggested the possibility of aromatic–aromatic side chain interaction between the invariant F425 in S5 and an aromatic substitution at position 480 in S6. Such an interaction would be energetically favorable (−1 to −2 kcal/mol; Burley and Petsko, 1985), and could stabilize a particular S5–S6 conformation from which the mutant channel may not enter a long-lived closed state. When the invariant F425 was mutated to alanine, the double mutants F425A/C480F and F425A/C480W showed a reduction in I_{SS}, a finding in agreement with aromatic–aromatic side chain interaction. We do not know why F425A-containing mutants with nonaromatic side chains at position 480 (F425A/C480, F425A/C480L, F425A/C480I, and F425A/C480H) and all tested F425I-containing mutants (F425I/C480, F425I/C480I, F425I/C480F, and F425I/C480W) did not result in functional K^+ channels in *Xenopus* oocytes.

Interestingly, using comparative sequence analysis, Durrell and Guy observed a cluster of correlated mutations involving the S5 and S6 residues that have been mutated in this study with a conserved position in S2 that is occupied by phenylalanine in EXP-2 and by tryptophan in most Kv-type K^+ channels (Guy, R., personal communication). If this cluster of correlated mutations reflected the physical proximity of the corresponding side chains then it would mean that the conserved aromatic residue in S2 should be close to and perhaps interact with S5 and S6. The invariant F425 in S5 could interact with the aromatic residue in S2 and contribute to tertiary structure stability (Burley and Petsko, 1985). Such a role of F425 would explain why most mutations at F425 did not lead to functional channels, and it would be in agreement with the notion that the introduction of an additional aromatic residue in S6 (e.g., C480F) could further stabilize a particular channel conformation through a network of aromatic–aromatic side chain interactions.

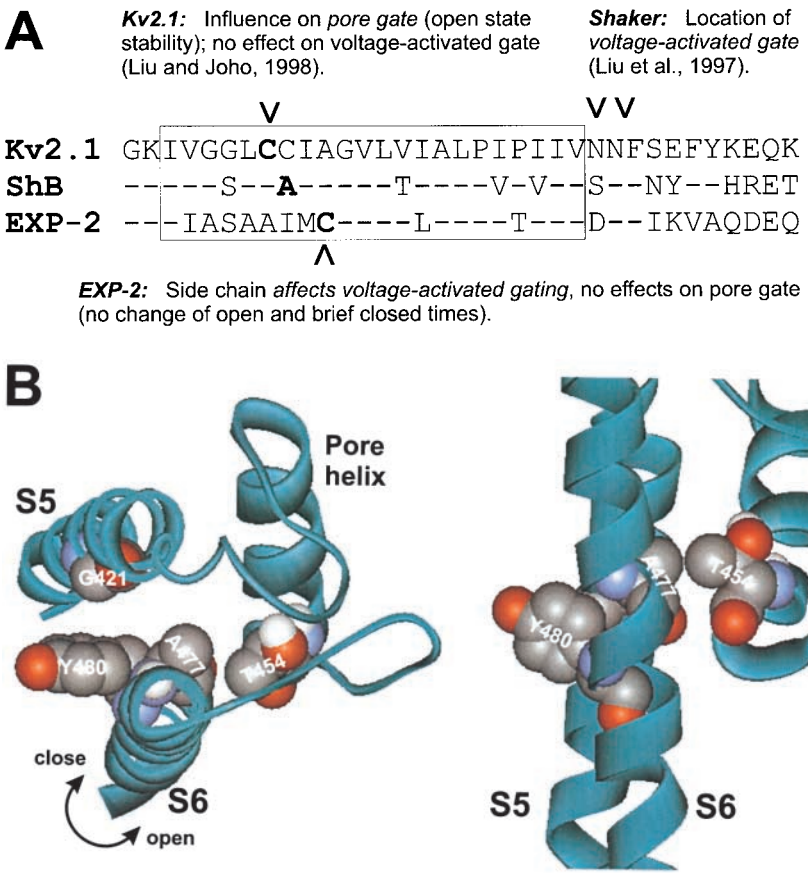

FIGURE 9. S6 Mutations in close proximity have opposite effects on channel gating. (A) The sequence alignment shows the similarity between Kv2.1, *Shaker* B (ShB) and EXP-2. The cysteine at position 393 in Kv2.1 (in bold) influences open-state stability and K^+/Rb^+ permeation (Liu and Joho, 1998); the nearest residue in *Shaker* (Hoshi et al., 1991) and in Kv1.3 (Panyi et al., 1995) determines the kinetics of C-type inactivation (in bold in the ShB sequence). The position of the EXP-2 mutations that prevent the channel from reaching long-lived closed states is three residues COOH-terminal from the Kv2.1 position that influences open-state stability (in bold in EXP-2 sequence). The approximate position of the voltage-activated gate in ShB (Liu et al., 1997) is shown by two downward arrowheads. (B) Top and side views of the C480Y EXP-2 mutant (modeled after KcsA) suggest how S6 residues that are only three positions apart may independently influence the voltage-activated gate and the voltage-independent pore gate. The bulky side chain Y480 prevents S6 rotation that is required for the channel to reach a long-lived closed state. In the open state, A477 (C393 in Kv2.1) is close to the conserved T454 (T370 in Kv2.1), which is located in the narrow ion conduction pathway (part of the K^+ channel signature sequence; Heginbotham et al., 1994). In Kv2.1, small hydrophilic side chains at position 393 in S6 (A477 in EXP-2) stabilize the open state and affect ion selectivity (Liu and Joho, 1998) presumably by interacting with T370 (T454 in EXP-2). In this model, substitutions for C393 in Kv2.1 (A477 in EXP-2) would only affect the stability of the open state as long as S6 is in the appropriate orientation for the side chain at position 393 to interact with T370. In the wild-type Kv2.1 channel, the interaction between T370 (T454 in EXP-2) and C393 (A477 in EXP-2) is broken when S6 rotates counterclockwise at negative membrane potentials. This rotation cannot occur in EXP-2 mutants with aromatic side chains at position 480 "trapping" the mutant channels in an open state without affecting open state stability (mean open time) or ion selectivity.

Mutant Channels Do Not Reach Long-lived, Stable Closed States

In contrast to the wild-type EXP-2 channel, which on recovery from inactivation shows a few bursts of single-channel activity and then enters a long-lived closed state at −80 mV, the mutant channels C480F and C480I maintain their bursting behavior at −80 mV (Fig. 7). The C480F and C480I mutants transition frequently to an open state (even after many seconds at −80 mV) that is of similar conductance like the one that is seen in the wild-type channel during the first 200 ms after recovery from inactivation (Fig. 7). Our results suggest that these mutant channels cannot reach long-lived, stable closed states. Due to mutations at positions 421 in S5 or 480 in S6, channels may enter a relatively unstable closed state from which they cannot proceed into a more stable, longer-lived closed state; hence, the channels often transition back into the open state leading to substantial current at potentials as negative as −160 mV.

In spite of the dramatic changes in the voltage-dependent closed-open transitions, mutations in S6 do not alter unit currents, suggesting no major structural alterations in the ion conduction pathway (the narrow pore) between wild-type and mutant channels. Furthermore, the open-time distributions of wild-type and mutant channels are similar (mean open times are ~0.2 ms; Fig. 8), indicating that the free energy of the open state is not changed by the S6 mutations at position 480 in spite of the dramatic effects on channel gating. Like the open-time distributions, the distributions for short closed times (in the millisecond range) are not changed between wild-type and mutant channels (Fig. 8). Hence, together with the finding that unit conductance (γ) is unchanged, it appears that the S6 mutations at position 480 exclusively affect the stable closing of the voltage-controlled activation gate located near the end of S6 (Liu et al., 1997), but that they neither influence K^+ permeation nor the fast open-closed state transitions. Although we cannot exclude other explanations, these findings agree with and support the notion that S5 and

S6 interact with each other, perhaps by rotation, during voltage-dependent channel gating, and that the perturbation of this interaction may prevent EXP-2 channels from reaching long-lived closed states.

Do Two Independent Gates Control Ion Permeation in Kv Channels?

Below, we will discuss our findings for EXP-2 in light of the "two-gate" model that we proposed for the voltage-gated K^+ channel Kv2.1 (Liu and Joho, 1998). The two-gate model postulates that a pore gate, located between the external and internal TEA-binding site, is responsible for the brief, voltage-independent openings and closings seen in single-channel records of Kv2.1. We proposed that the pore gate interacts with the conserved cysteine in S6 of Kv channels (C393 in Kv2.1) because subtle, conservative substitutions for C393 dramatically affect both ion permeation and open state stability but have no effect on blockade by external or internal TEA (Liu and Joho, 1998; Fig. 9). Small hydrophilic side chain substitutions at position 393 stabilize the open state, whereas larger side chains destabilize the open state; however, these S6 mutations in Kv2.1 have little or no effect on voltage-dependent gating, i.e., on the movement of the voltage-controlled activation gate located near the end of S6 (Liu et al., 1997).

The S6 mutations at position 480 in EXP-2 appear to have the opposite effect compared with the S6 mutations in Kv2.1. The EXP-2 mutations only affect the voltage-activated gate (no permanent, stable closing at negative potentials) but have no effect on the pore gate (no changes in open or intraburst closed times). In EXP-2, the mutations are located three residues from the position in Kv2.1 (C393) involved in stabilizing the open state and two residues from the position involved in C-type inactivation in *Shaker* (A463; Hoshi et al., 1991) and Kv1.3 (A413; Panyi et al., 1995). Although it is surprising that mutations located in such close proximity yield mutant channels with vastly different gating properties, a possible mechanism explaining this finding is described in Fig. 9 B.

Our two-gate model for Kv channel gating can be tested. The introduction of small, hydrophilic side chains at position 477 in S6 of EXP-2 (corresponding to C393 in Kv2.1) should result in longer open times and influence ion permeation, without affecting brief closed times and the voltage-activated gating process; the presence of larger side chains may result in even shorter open times than seen in wild-type EXP-2. Conversely, the introduction of large side chains at position 396 in S6 of Kv2.1 (corresponding to C480 in EXP-2) may prevent Kv2.1 channels from reaching stable closed states without changing open times and ion permeation.

The authors would like to thank Drs. Alan Neely, Ege Kavalali, and Robert Guy for helpful suggestions and insightful discussions and Dr. Donald Hilgemann for critical input to the manuscript.

This work was supported in part by the National Institutes of Health grant No. NS28407 to R.H. Joho.

Submitted: 15 March 2001
Revised: 26 June 2001
Accepted: 27 June 2001

REFERENCES

Burley, S.K., and G.A. Petsko. 1985. Aromatic-aromatic interaction: a mechanism of protein structure stabilization. *Science.* 229:23–28.

Davis, M.W. 1999. Regulation of the relaxation phase of the *C. elegans* pharyngeal muscle action potential. Ph.D. dissertation. The University of Texas Southwestern Medical Center at Dallas. Texas. 119 pp.

Davis, M.W., R. Fleischhauer, J.A. Dent, R.H. Joho, and L. Avery. 1999. A mutation in the *C. elegans* EXP-2 potassium channel that alters feeding behavior. *Science.* 286:2501–2504.

Doyle, D.A., J. Morais Cabral, R.A. Pfuetzner, A. Kuo, J.M. Gulbis, S.L. Cohen, B.T. Chait, and R. MacKinnon. 1998. The structure of the potassium channel: molecular basis of K^+ conduction and selectivity. *Science.* 280:69–77.

Fleischhauer, R., M.W. Davis, I. Dzhura, A. Neely, L. Avery, and R.H. Joho. 2000. Ultrafast inactivation causes inward rectification in a voltage-gated K^+ channel from *Caenorhabditis elegans. J. Neurosci.* 20:511–520.

Guex, N., and M.C. Peitsch. 1997. Swiss-model and the Swiss-PDB viewer: an environment for comparative protein modeling. *Electrophoresis.* 18:2714–2723.

Heginbotham, L., Z. Lu, T. Abramson, and R. MacKinnon. 1994. Mutation in the K^+ channel signature sequence. *Biophys. J.* 66: 1061–1067.

Hoshi, T., W.N. Zagotta, and R.W. Aldrich. 1991. Two types of inactivation in *Shaker* K^+ channels: effects of alterations in the carboxy-terminal region. *Neuron.* 7:547–556.

Liu, Y., and R.H. Joho. 1998. A side chain in S6 influences both open-state stability and ion permeation in a voltage-gated K^+ channel. *Pflügers Arch.* 435:654–661.

Liu, Y., M. Holmgren, M.E. Jurman, and G. Yellen. 1997. Gated access to the pore of a voltage-dependent K^+ channel. *Neuron.* 19: 175–184.

Moorman, J.R., G.E. Kirsch, A.M.J. VanDongen, R.H. Joho, and A.M. Brown. 1990. Fast and slow gating of sodium channels encoded by a single mRNA. *Neuron.* 4:243–252.

Panyi, G., Z. Sheng, L. Tu, and C. Deutsch. 1995. C-type inactivation of a voltage-gated K^+ channel occurs by a cooperative mechanism. *Biophys. J.* 69:896–903.

Perozo, E., D.M. Cortes, and L.G. Cuello. 1999. Structural rearrangements underlying K^+-channel activation gating. *Science.* 285:73–78.

VanDongen, A.M.J., G.C. Frech, J.A. Drewe, R.H. Joho, and A.M. Brown. 1990. Alteration and restoration of K^+ channel function by deletions at the N- and C-termini. *Neuron.* 5:433–443.

Zühlke, R.D., H.J. Zhang, and R.H. Joho. 1994. Role of an invariant cysteine in gating and ion permeation of the voltage-sensitive K^+ channel Kv2.1. *Recept. Channels.* 2:237–248.

Zühlke, R.D., H.J. Zhang, and R.H. Joho. 1995. *Xenopus* oocytes: a system for expression cloning and structure-function studies of ion channels and receptors. *Methods Neurosci.* 25:67–89.